MODIFICATION OF TURBULENT BOUNDARY LAYER STRUCTURE USING IMMERSED WALL-MOUNTED CYLINDERS

Cecilia Ortiz-Dueñas
Institute for Mathematics and its Applications
University of Minnesota, Minneapolis, MN, 55455, USA
cecilia@ima.umn.edu

Mitchell D. Ryan
Department of Aerospace Engineering and Mechanics
University of Minnesota, Minneapolis, MN, 55455, USA
ryanx439@umn.edu

Ellen K. Longmire
Department of Aerospace Engineering and Mechanics
University of Minnesota, Minneapolis, MN, 55455, USA
ellen@aem.umn.edu

ABSTRACT

Spanwise arrays of wall-mounted cylinders with $H/\delta \leq 0.2$, where H is the cylinder height and δ is the boundary layer thickness, and tall enough to protrude into the logarithmic region were used to modify turbulent boundary layers (Re_τ=2400) in an attempt to affect the organization of the coherent vortical structures. Velocity fields were obtained downstream of the arrays by PIV and V3V. Averaged results yielded initial splitting and divergence of wakes downstream of cylinders followed by consistent initial pairing of neighboring wake structures at a location that scaled with the array spacing. Perturbation effects were limited to the log region. Instantaneous results showed that an array with 8D (0.4δ) spacing yielded relatively stable, long low speed regions while an array with 4D (0.2δ) spacing typically yielded additional pairings and a greater variability in spanwise location of downstream structures.

MOTIVATION

In practical applications, it may be desirable to manipulate boundary layers in order, for example, to improve aerodynamic or combustion performance, locally increase or decrease skin-friction or heat transfer, or reduce noise. Since coherent vortical structures or eddies are believed to be a key self-sustaining mechanism in wall bounded turbulence (Panton, 2001). A possible method to manipulate the behaviour of turbulent boundary layers is to alter or modify these coherent structures or their organization.

In the current investigation, arrays of wall-mounted cylinders, smaller than the boundary layer thickness but large enough to protrude into the logarithmic region, are used to attempt to manipulate the structure of turbulent boundary layers. The PIV studies by Adrian et al. (2000), Ganapathisubramani et al. (2003) and Tomkins and Adrian (2003) served as guidelines for the wall-normal and spanwise scaling of the arrays that might potentially result in more efficient manipulation of turbulent boundary layers. For instance, Adrian et al. (2000) and Tomkins and Adrian (2003) demonstrated the preponderance of hairpin signatures in both the logarithmic and outer regions. The signature pattern consists of vortex cores with high values of swirling strength organized coherently in the streamwise direction in groups or packets above regions with high Reynolds shear stress, $u'v'<0$, and low speed, $u'<0$ (Tomkins and Adrian, 2003 and Ganapathisubramani et al., 2003). Ganapathisubramani et al. (2003) also found that the spanwise spacing of packets in the log region at Re_τ =1150 is of order 0.3-0.7δ while the packet width is approximately 0.15-0.2δ. Similarly, Tomkins and Adrian (2003), found that at Re_τ =2216 also in the log region, the spanwise spacing is 0.5-1.0δ and the packet width is 0.2-0.4δ. From these studies it appears that, starting in the log layer, the packet spacing may scale on the boundary thickness.

Based on these studies, the logarithmic region, where hairpins and streamwise-oriented hairpin packet signatures are prevalent, appears to be of particular interest. Moreover, the spanwise spacing and width of packets in the log region, approximately 0.2δ and 0.5δ respectively, appear to be naturally occurring scales. Since our goal is to perturb the structure in this region, we are interested in wall-mounted obstacles that reach into the logarithmic region but not beyond, e.g. a sparse array arranged in a single spanwise row with array spacings on the order of tenths of the boundary layer thickness.

The sparseness of the single row of wall-mounted cylinders used in this investigation yields a flow field that differs significantly from that over roughness elements or canopy flows and therefore studies related to these types of obstructions are not reviewed here. On the other hand, investigations of single or rows of wall-mounted cylinders immersed within a turbulent boundary layer are relatively few, and the majority of these studies focus on the detailed flow downstream of a single cylinder for $x/D \leq 5$, where x is the streamwise coordinate. For example, Sumner et al. (2004) found that for cylinders with constant diameter ($Re_D \sim 6x10^4$

based on freestream velocity) and AR≤2-3, corresponding in their case to H/δ < 1.2, the resulting downwash from the tip vortex suppresses both the Karman-type and horseshoe vortices. Wang et al. (2006) also observed that for flow past cylinders at Re_D~1.1x10^4 and with aspect ratio larger than 3-4, corresponding to H/δ>>1, the effects of the free-end shear layer are confined to the tip region so that the near-wake is dominated by Karman-type vortices and horseshoe vortices. Thus, it appears that for the cylinders investigated herein with relatively low aspect ratios, the free-end shear layer and any resulting tip vortices would have an effect on the near downstream flow field. In turn, the height of the cylinder with respect to the boundary layer thickness, H/δ, will affect the development of the wake structures. Wang et al. (2006) found that the strength of the horseshoe vortex system (in particular the downwash directly behind a rod) was shown to increase with decreasing H/δ (H/δ=5 and 2.63). Similar results were obtained by Sakamoto and Arie (1983) and Park and Lee (2002) for Re_D~2-4x10^4 based on freestream velocity. In contrast, Castro and Robins (1977) investigated the near wake (x/D<5) behind a cube with H/δ=0.1 and Re_H~4x10^3 based on freestream velocity embedded in a turbulent boundary layer. They found that as H/δ was increased above 0.1, such that the upstream turbulence intensity at height H was decreased, the length of the recirculation zone behind the cubes increases; this effect is due to the larger separated shear layers on the top and sides of the cube as inferred by the authors from pressure measurements. Tomkins (2001) investigated the flow downstream (x/D≤10) of single cylinders and hemispheres with AR<2, H/δ≈0.05-0.15 (H^+≈100-300) and Re_D~5x10^3 based on freestream velocity, that were entirely immersed in the logarithmic region of a turbulent boundary layer. Tomkins (2001) concluded that even though the peak of swirling strength measured downstream occurs at approximately mid-height for all elements, a significant swirling strength is observed downstream of the hemisphere for heights up to 2H or H^+≈400, which corresponded to approximately the top of the log region. Furthermore, the author found that the upstream turbulence disrupted shedding frequency such that no dominant frequency was measured. It is clear from these studies that firstly the flow past a cylinder entirely immersed in a turbulent boundary layer differs significantly from the flow past a cylinder that extends beyond the boundary layer thickness δ. And secondly that the turbulent boundary layer and the flow generated by the cylinder will affect each other significantly.

Table 1. Turbulent boundary layer properties.

	U (m/s)	δ (mm)	$\mathbf{u_\tau}$ (mm/s)	Re_θ	Re_τ
Water Channel, Stereo PIV	0.51	125.5	19.8	6150	2480
Water Channel, V3V (FF)	0.49	134.4	18	7050	2410
Water Channel, V3V (NF)	0.51	128.5	19.2	6150	2460

The goal of the current investigation is to manipulate or alter the structure of a turbulent boundary layer by inserting single spanwise arrays of cylinders into the log region. The wall-mounted cylinders, with an aspect ratio AR=1.5, are fully immersed within the turbulent boundary layer such that they extend well into the log region, H/δ=0.13 (H+=150). Two array spacings were investigated: Δy/δ =0.2 (4D) and Δy/δ =0.4 (8D). The effect on the mean and instantaneous flow fields downstream of the arrays up to approximately x/δ=4 are investigated with a focus on understanding the interaction of the flow generated downstream of the cylinders with the structure of the turbulent boundary layer.

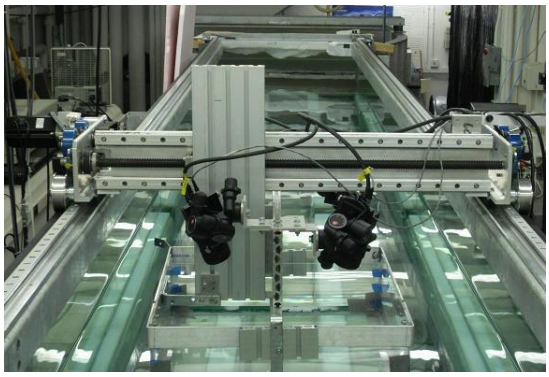

Figure 1. Water channel facility.

APPROACH

Measurements were carried out in a zero pressure gradient boundary layer using a recirculating water channel shown in Figure 1. Properties of the turbulent boundary layer in this facility are summarized in Table 1. Hot wire measurements were taken previously in a suction type, zero-pressure gradient wind tunnel for lower Reynolds number and multiple cylinder arrays. These measurements and the facility are described in detail in Ryan et al. (2011). The wall shear stress, τ_w, in each facility was obtained using the Clauser chart method and the mean velocity profile for the unobstructed case, i.e. with no cylinder arrays. All quantities denoted with the superscript + are thus normalized using the wall friction velocity $u_\tau=(\tau_w/\rho)^{1/2}$ for the unobstructed case and the kinematic viscosity ν for each corresponding facility.

In these investigations, a single spanwise array of cylinders was used as an obstacle. Cylinders were chosen as obstacles because of their relatively simple geometry. The

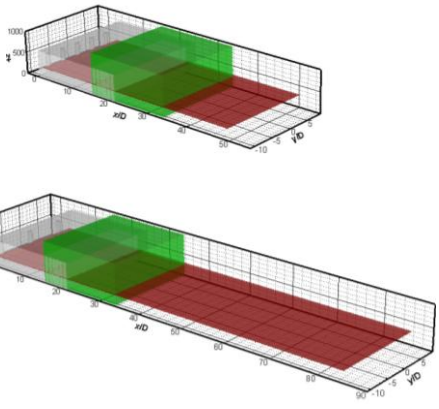

(a)

(b)

Figure 2. Water channel facility measurement regions normalized by cylinder diameter for (a) the cylinder array with 4D spanwise spacing (b) the cylinder array with 8D spanwise spacing. Red plane: Stereo PIV, Grey Volume: Near field V3V, Green Volume: Far field V3V

cylinders, stainless steel smooth dowel pins, were attached to the facility floor using a drop of glue. The cylinder height was selected such that the corresponding H^+ was within the logarithmic region and thus within the zone containing the bulk of the coherent eddies. The cylinders were also selected to have a low blockage ratio (ratio of the frontal area of the cylinders to the boundary layer cross-sectional area) and thus the aspect ratio of the cylinders (AR = H/D, where D is the cylinder diameter) is larger than one. In the investigation presented here, two spanwise spacings were studied: 4D and 8D center-to-center spacing. The geometrical parameters for these arrays are summarized in Table 2. The Reynolds number based on cylinder diameter and mean velocity at 2/3 of the cylinder height for these arrays is of order 2300.

Table 2. Cylinder Arrays

Obstacle	H/δ	H/D	H^+	Spanwise Spacing	Re_D
Cylinder Array	0.19	4	455	4D (0.2δ)	2300
Cylinder Array	0.19	4	455	8D (0.4δ)	2300/2500

Measurements downstream of cylinder arrays were carried out using two experimental techniques. Firstly, stereo PIV was used to examine wall-parallel planes at a series of downstream locations at z^+=296 (0.67H), illustrated in red in Figure 2. Secondly, a Volumetric 3-Component Velocimetry (V3V) system was used to obtain three-component velocity measurements within specific volumes, illustrated as grey and green in Figure 2.

For the Stereo-PIV measurements, the flow was seeded with 10μm silver-coated hollow glass spheres and illuminated with 1 mm thick sheets from a Spectra-Physics Nd:YAG laser with 350 mJ/pulse. Two 12-bit 2048 x 2048 pixel CCD cameras arranged in the spanwise direction and angled approximately 15° from the vertical (z axis) were used to image a ~152mm x 152mm field from above. A window size of 32 x 32 pixels, corresponding to a spatial resolution of 2.4mm, was used with 50% overlap for correlation processing. These measurements were obtained at a wall normal distance of z^+=296 (0.67H) spanning a distance from just upstream of the cylinders to x/D=50 for the 4D array spacing and to x/D=85 for the 8D array spacing.

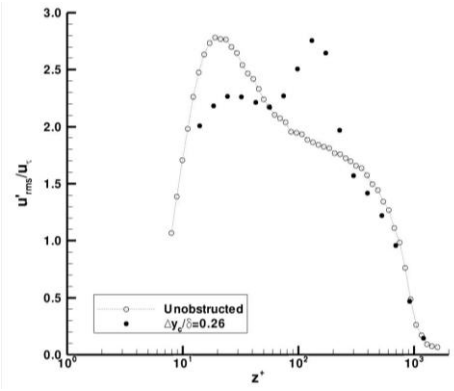

Figure 3. Streamwise r.m.s. velocity at midspacing at x/δ=1.0 downstream of cylinder array with 0.26δ spacing compared with unobstructed profile at Re_τ=1150. Hot wire measurements.

For the V3V measurements, flow, seeded with 60μm (far field measurements) and 10μm silver (near field measurements) silver coated hollow glass spheres, was illuminated by thick laser sheet and captured using a 3-aperture camera probe placed below the water channel. In this study, the volume of interest (120 x 120 x 50 mm^3) was placed at $52<z^+<1000$ and $0.8<x/\delta<1.6$. Measurements were conducted downstream of each cylinder array at streamwise locations of $1<x/D<21$ ('Near Field') and $15<x/D<35$ ('Far Field'). As with the stereo PIV, the undisturbed flow was also measured using this technique, and mean and rms statistics matched well with independent LDV measurements.

The uncertainty of the mean and rms velocities reported here based on sample size was less than $0.5u_\tau$ of the reported values respectively. The uncertainty in instantaneous velocity measurements due to a pixel precision of 0.1pixels was less than 5% for all measured velocities after filtering outlier vector.

RESULTS

Figure 1 shows two profiles of streamwise r.m.s. velocity including an undisturbed profile and a profile at mid-spacing downstream of a cylinder array with spanwise spacing of

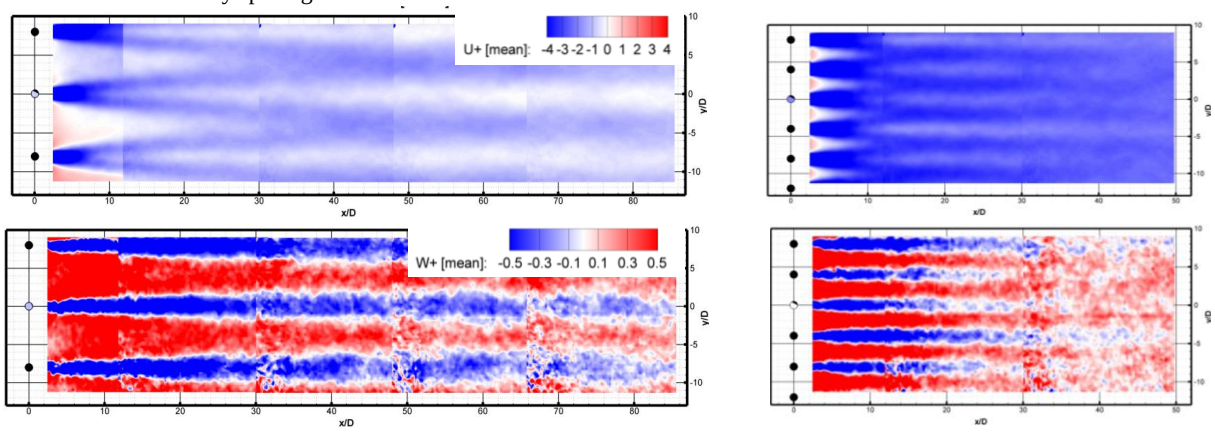

(a) (b)

Figure 4. Mean streamwise (top) and wall-normal (bottom) velocity fields at z^+=293 obtained by stereo PIV. Flow is from left to right. Mean unperturbed fields are subtracted. (a) Spanwise Spacing = 0.4δ (8D) and (b) Spanwise Spacing = 0.2δ (4D).

0.26δ. These profiles were obtained in earlier experiments at Re_τ=1150 and at a streamwise distance of x/δ=1.0 from the cylinder array via hot wire anemometry (see Ryan et al., 2011). The profiles reveal a redistribution of turbulence intensity away from the near-wall region (z^+≈20) towards the cylinder-height (H^+=150) which corresponds approximately to the top of the log region. If the spanwise array spacing was increased, a similar but weaker effect was observed; if spanwise spacing was decreased, the effect became stronger. For the higher Reynolds number boundary layer presented here (Re_τ=2480), a similar redistribution towards the top of the cylinder (H^+=455, corresponding to the top log region) was also observed; even when accounting for increases in streamwise r.m.s. velocity due to the Reynolds number increase (DeGraaff and Eaton, 2000). At both Reynolds numbers, the perturbations to the velocity field (mean and r.m.s.) were observed to extend only to the top of the log region for each Reynolds number, even for cylinders with half of the original height. This scaling was also observed by Tomkins (2001) for single obstacles embedded in a boundary layer with Re_τ=2200.

Averaged Flow

The consistent perturbations to the velocity field observed in the earlier hot wire data suggest significant interaction between the cylinder wakes and the incoming turbulent boundary layer. To investigate this interaction in detail, streamwise-spanwise planes were obtained for up to several boundary layer thickness downstream of arrays with spanwise spacings of 0.2δ and 0.4δ at Re_τ=2480. These streamwise-spanwise planes (see Figure 2) were located at z^+=293, the location of maximum streamwise r.m.s. velocity for this Reynolds number (a larger z^+ than for Re_τ-1150 in Figure 1).

Figure 4 shows mean streamwise velocity with respect to the undisturbed values for these streamwise-spanwise planes. Directly downstream of each cylinder, an initial wake is evident as a streamwise velocity deficit (blue in Figure 4). However, each wake proceeds to split in two, and the two halves move apart with increasing downstream distance until each one interacts with its neighbour. Adjacent 'split' wakes then appear to pair. For the array with 8D spacing, the pairing occurs at x=32D (1.6δ). In contrast, for the array with 4D spacing, the pairing occurs at x=12D (0.6δ). Thus, for both arrays the wake pairing occurs at a downstream distance of 3-4 array spacings. After this pairing, the resulting spacing between wakes persists over a long distance: to x = 50D for the 4D array and to x/D = 90 (4.4δ) for the 8D array. The incomplete spanwise mixing of the wakes results also in non-uniform wall-normal velocity distributions as shown also in Figure 4. The mean wall-normal velocity becomes almost uniform downstream of the 4D array (x/D = 50), but not downstream of the 8D array (up to x/D = 90). This difference was observed also in the mean spanwise velocity fields (not shown). Together, these results suggest that the perturbations in the mean field downstream of the 8D array are more stable, i.e. persist for longer streamwise distances in all velocity components. Thus, this scale (0.4δ=8D) appears to have a larger effect on the development and structure of the turbulent boundary layer.

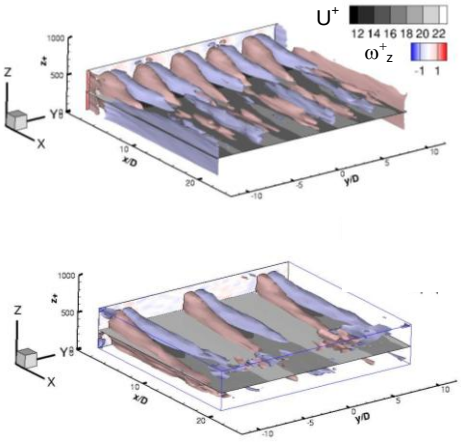

Figure 5. Iso-surfaces of wall-normal vorticity, ω_z within a volume located at 1<x/D<20, -10<y/D<10, and 40<z+<570. Plane at z^+=273 shows grey-scale contours of mean streamwise velocity.

V3V measurements were used to study the volumetric flow field behind the cylinders and how its development relates to the relative stability of the wake pairings observed. Based on the literature, it is likely that the flow field would include three features: the tip vortex at the free end of the cylinder (generating both streamwise and spanwise vorticity, ω_x and ω_y), the wake shed from the body of the cylinder (identified by wall-normal vorticity ω_z) and a horseshoe vortex system along the base of the cylinder (identified by streamwise vorticity). The relative strength of each of these features was compared using the vorticity components available from the volumetric velocity fields.

The average spanwise components from tip vortices and the horseshoe vortex system, which were confined to regions

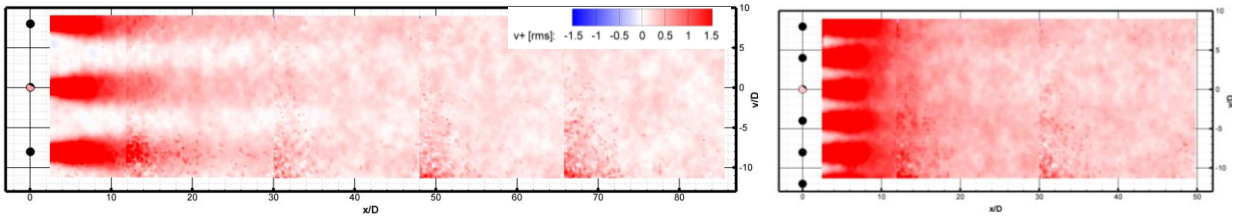

(a) (b)

Figure 6. Spanwise r.m.s. velocity at z^+=293 obtained by stereo PIV. Flow is from left to right. Mean unperturbed fields are subtracted. (a) Spanwise Spacing = 0.4δ (8D) and (b) Spanwise Spacing = 0.2δ (4D).

very near the cylinders, approximately x/D<3, were significantly smaller in magnitude than other vorticity components. Therefore, they did not appear to have a significant effect on the mean flow field further downstream. This is opposite to what might be expected based on the previous literature for flow behind low aspect ratio cylinders (Sumner et al., 2004), and is most likely due to the presence of surrounding turbulence. Streamwise vorticity caused by tip vortices, which has opposite sign along each side of the cylinders was observable for x/D ≤ 10-12 for both arrays, independent of whether wake pairing had occurred or not. This result suggested that neighboring tip vortices did not interact regardless of the array spacing or wake pairing, at least for the spacings investigated here.

The most interesting component of vorticity, in terms of its development along the volume, was the wall-normal vorticity ω_z plotted in Figure 5 as iso-surfaces within volumes extending over the range 40<z+<570 (the cylinder height was 455 wall units). The wake pairing can be observed via grey scale contours of streamwise velocity plotted on streamwise-spanwise planes at z^+=273. In this figure, the organized wall-normal vorticity persists through the volume beyond the pairing locations as might be expected from the earlier wake patterns.

As observed in Figure 4, the cylinder wakes initially split into two weaker, narrower wakes diverging away from the centerline of the cylinder body. This is clearly different from the behavior expected behind a long cylinder outside of a boundary layer region in which the maximum velocity deficit remains directly behind the cylinder while the wake widens with increasing distance downstream. Directly downstream of each cylinder, the mean wall-normal velocity is negative; indicating that relatively faster moving flow is being pulled downwards towards the wall. This concept is consistent with the streamwise contours in Figure 4 where the streamwise velocity directly behind each cylinder becomes higher than midway between the cylinders. The infusion of faster moving flow also generates spanwise velocity gradients which result in wall-normal vorticity with opposite direction to that generated originally behind each cylinder. As downstream distance increases, the split cylinder wakes encounter neighbouring split wakes with opposite rotation. The flow interaction just described was identified earlier as wake pairing. The 'new' paired wake is identified clearly by wall-normal vorticity patterns opposed to those originally generated. In Figure 5, this causes a spanwise shift in the location of a given vorticity sign, e.g. blue, near the pairing location behind the array with 4D spacing. Figure 4 shows that as downstream distance increases, the velocity deficit of this paired wake increases initially compared to the unpaired wake upstream, possibly because of local upwash in this region.

The question remains as to why the paired wakes appear to persist over longer streamwise distances for the array with 8D spacing. The mixing out of the wakes will depend, not only on mean gradients, but also on the instantaneous structure within the boundary layer. Spanwise r.m.s. velocity fields are shown in Figure 6. The closer proximity of the cylinders in the 4D array results in stronger average fluctuations (as shown by the darker red contours) than in the 8D array case and the unperturbed case (not shown). Note that the strongest fluctuations occur directly behind the cylinders and no effect of pairing is observable. However, in the 4D array case, the fluctuation levels become relatively uniform in the spanwise direction already by x/D = 20. For the 8D array case, the spanwise variations are distinct until x/D ≈ 48. The stronger fluctuations in the 4D array case could be caused by either a range of eddies convecting past a given location or wake-like structures meandering in the spanwise direction. As will be shown below, the earlier spanwise uniformity downstream of the 4D array is most likely a result of additional wake pairing.

Instantaneous Flow

Instantaneous velocity fields obtained via stereo PIV were examined to investigate the wake pairing effect. Four instantaneous stereo PIV fields are shown in Figure 7. The instantaneous fields cover a streamwise distance of up to 8 array spacings for each array. Both streamwise velocity and two-dimensional swirl (λ_{2D}) are plotted. The swirl is used to identify cores of eddies or vortices crossing the measurement plane. For x/D<14, the locations of low speed regions and

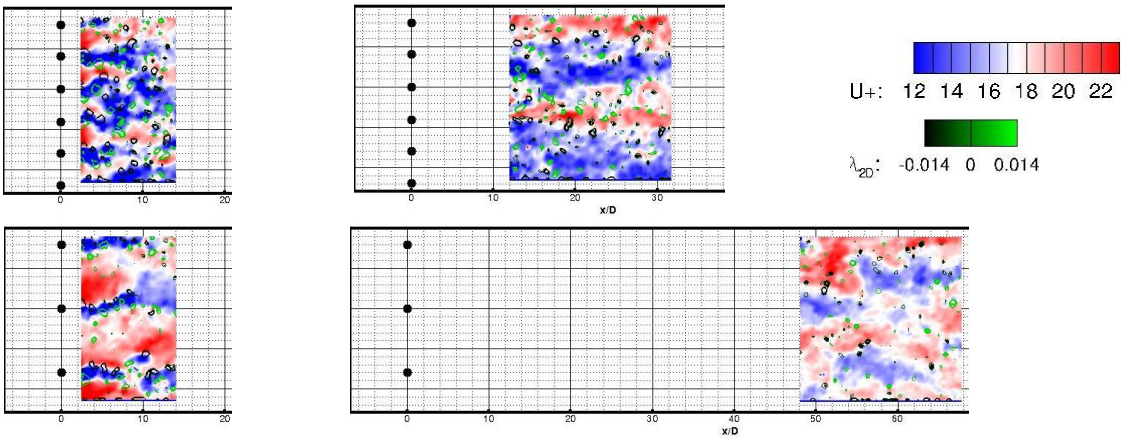

Figure 7. Instantaneous planes downstream of each array. Contours of streamwise velocity with contour lines of signed two-dimensional swirl (λ_{2D}) overlapped.

swirling structures bounding these regions occur consistently directly downstream of the cylinders (for both arrays). However, farther downstream, the instantaneous fields appear quite different from the mean field. Downstream of the 4D array, the spanwise location of low speed regions and accompanying swirling structures varies significantly, and their spanwise spacing varies from 0.2δ to greater than 0.4δ. This could explain the higher r.m.s. values observed in the mean fields in Figure 7. Downstream of the array with 8D spacing, meandering in the spanwise direction of low speed regions is evident but their spanwise separation appears to be more stable and scale with the 8D spacing (0.4δ) or a slightly larger spacing, e.g. 0.6δ-0.8δ. Therefore, future studies will examine even larger cylinder spacings as potentially more stable.

CONCLUSIONS

The goal of the current investigation is to manipulate or alter the structure of a turbulent boundary layer by inserting single spanwise arrays of cylinders into the log region. Two array spacings were investigated: $\Delta y/\delta$ =0.2 (4D) and $\Delta y/\delta$ =0.4 (8D). It was found that a single array of cylinders could significantly affect both the mean and instantaneous flow behaviour in a turbulent boundary layer in a consistent manner for a long distance downstream. In particular, the following was observed:

- Adjacent wakes initially split but then pair at a downstream distance which scales with the spanwise spacing.
- In the log region, the dominant vorticity components are both streamwise and wall normal. However, any mean streamwise vortices appear to die out by x/D = 10 for both arrays.
- The array with 8D spacing (0.4δ) yielded a single pairing followed by a relatively stable spacing of 0.4δ between low speed structures. Observation of instantaneous fields suggested that the most stable spacing may be higher, e.g. 0.6δ-0.8δ. Instantaneous fields downstream of the array with 4D spacing (0.2δ) suggested that the initial pairing was followed by at least one additional pairing. In this case, spanwise variability and meandering of low speed structures yielded r.m.s. fields with higher values overall and relative uniformity across the span for x/D > 34.

Future work includes detailed studies on the evolution of the instantaneous structures and their relation to hairpin packets present in unperturbed fields.

ACKNOWLEDGEMENTS

The authors gratefully acknowledge support from NSF through Grant CBET-0933341 and from Institute for Mathematics and its Applications at University of Minnesota.

REFERENCES

Adrian, R. J., Meinhart, C. D., and Tomkins, C. D., (2000), "Vortex organization in the outer region of the turbulent boundary layer", *J. Fluid Mechanics*, 422, pp. 1-54.

Adrian, R. J., and Tomkins, C. D., "Spanwise structure and scale growth in turbulent boundary layers", *Journal of Fluid Mechanics,* Vol. 490, September 2003, pp. 37-74.

Castro, I. P., Cheng, H., and Reynolds, R., "Turbulence over urban-type roughness: deductions from wind-tunnel measurements," *Boundary-Layer Meteorology,* Vol. 118, No. 1, 2006, pp. 109-131.

Castro, I. P., and Robins, A. G., "The flow around a surface-mounted cube in uniform and turbulent streams," *Journal of Fluid Mechanics,* Vol. 79, February 1977, pp.307-335.

Coceal, O., Dobre, A., Thomas, T. G., and Belcher, S. E., "Structure of turbulent flow over regular arrays of cubical roughness," *J. Fluid Mech.,* Vol. 589, 2007, pp. 375-409.

De Graaff, D. B. and Eaton, J. K., (2000), Reynolds-number scaling of the flat-plate turbulent boundary layer. *Journal of Fluid Mechanics*, 422, pp 319-346.

Ganapathisubramani, B., Longmire, E. K., and Marusic, I., (2003), "Characteristics of vortex packets in turbulent boundary layers," *J. of Fluid Mechanics*, 478, pp. 35-46.

Panton, R. L., (2001), "Overview of the self-sustaining mechanisms of wall turbulence", *Progress in Aerospace Sciences*, Vol. 37, No. 4, pp. 341-383.

Park, C. W., and Lee, S. J., "Flow structure around a finite circular cylinder embedded in various atmospheric boundary layers," Fluid Dynamics Research, Vol. 30, No. 4, 2002, pp. 197-215.

Ryan, M. D., Ortiz-Dueñas C, and Longmire, E. K "Effects of Simple Wall-Mounted Cylinder Arrangements on a Turbulent Boundary Layer", *AIAA Journal,* in press.

Sakamoto, H., and Arie, M., "Vortex shedding from a rectangular prism and a circular cylinder placed vertically in a turbulent boundary layer," *Journal of Fluid Mechanics*, Vol. 126, January 1983, pp. 147-165.

Sumner, D., Heseltine, J. L., and Dansereau, O. J. P., "Wake structure of a finite circular cylinder of small aspect ratio," *Experiments in Fluids*, Vol. 37, No. 5, 2004, pp. 720-730.

Tomkins, C. D and Adrian, R. J., (2003) "Spanwise structure and scale growth in turbulent boundary layers", *Journal of Fluid Mechanics*, 490, pp 37-74.

Tomkins, C. D., (2001), "The Structure of Turbulence Over Smooth and Rough Walls.", PhD Thesis, University of Illinois at Urbana-Champaign

Wang, H. F., Zhou, Y., Chan, C. K., and Lam, K. S., "Effect of initial conditions on interaction between a boundary layer and a wall-mounted finite-length-cylinder wake," *Physics of Fluids*, Vol. 18, No. 6, June 2006, 065106.

Williamson, C. H. K., "Vortex Dynamics in the Cylinder Wake," *Annual Review of Fluid Mechanics*, Vol. 28, January 1996, pp. 477-539.

Zhou, Y., Zhang, H. J., and Yiu, M. W., "The turbulent wake of two side-by-side circular cylinders," *J. Fluid Mechanics*, Vol. 458, May 2002, pp. 303-332.